Chapter 3

Slope of the lateral density function of electron distribution in extensive air showers

3.1 Introduction

The origin of high-energy CRs remains a long existing question in astro-particle physics since after their discovery in 1912. This situation is in part due to the inadequate knowledge of the nature and the spectra of energetic primary cosmic rays (PCRs) from their direct measurements above a few 10^{14} eV. Even the presently available sophisticated technology, viz. satellites and balloon borne experiments, cannot do the job because of the very low flux of the radiation. Currently the only feasible way to get information about such energetic particles is through the study of CR EAS which are cascades of many secondary particles produced when PCR particles interact with atmospheric nuclei during their advancement towards the ground.

There exists a power law behavior in the energy spectrum of PCRs with three breaks. First, a 'knee' around 3 PeV just after which the spectral index suddenly takes a value -3.1 from -2.7. Secondly, an 'ankle' in the vicinity of the few EeV energy after which the spectrum flattens again to its original slope. Finally, at energies above 4×10^{19} eV, the PCR flux experiences a suppression which is compatible with the GZK effect. However, other possible reasons (e.g. upper limit in the energy at the source) for the suppression cannot be ruled out. Present

understanding takes the knee to be a signature of galactic origin of PCRs. Hence, measurements of several characteristics of PCRs including its mass composition around the knee are very important for proper understanding of the origin of this spectral feature.

Observables from EAS experiments are known to be densities and arrival times of cascade particles. More than 90% of the various charged secondaries are sum of e^- and e^+. These observables are measured at different radial distances, and they contain all information on the primary particle. By applying the shower reconstruction to the electron density data using the so called NKG type LDF, the crucial EAS parameters such as $N_{\rm e}$, the EAS core and the s are obtained. The observed results are usually interpreted by means of detailed MC simulations which cautiously account various interaction processes of primary or a few secondary particles as input. But our understanding of hadronic interactions at high energies is limited. In addition, there exists huge fluctuations in interaction mechanisms in a cascade which however are intrinsic to any EAS. Therefore, any conclusion derived from EAS measurements remains somewhat uncertain, and even sometimes there are huge inconsistencies on conclusions drawn from the experiments. Therefore, a multi-observable approach in this context is expected to be more efficient. In this approach, several possible EAS parameters are simultaneously considered in order to extract information on shower initiating primaries in EAS experiments with smaller uncertainties.

In this chapter, the shower age , which is directly linked to the slope of the LDF (NKG), and essentially describes the form or shape of the lateral distribution of EAS electrons, is adjudged an important parameter in the multi-parameter approach. It provides the fundamental relation between the depth of shower maximum ($X_{\rm max}$) and the slope of the LDF. It also determines the stage of shower development, starting mainly from the depth of shower maximum point to the ground as per electromagnetic (EM) cascade theory. Hence, the value of s is related to the degree of steepness of the lateral distribution of electrons. By virtue of these features of the s parameter, it is still being used to study the PCRs.

We organize the chapter as follows. In the next section (section 3.2), we discuss how the concept of shower age, introduced in the EM theory, is used to describe the evolution of an EAS in the longitudinal and transverse (i.e. lateral) directions

with respect to the shower axis in the atmosphere. In section 3.3, the characteristics of the method of simulation used in this work will be described. The same section also includes the method of analysis of simulated data for estimation of air shower parameters. The results of the study are presented in section 3.4 with the necessary discussion. Conclusions will be drawn in section 3.5.

3.2 The concept of shower age describing the extensive air shower development

The concept of the shower age has been used in CR studies since around 1940. It first appears in the early works of Rossi and Greisen [1], and later in Nishimura's work [2]. Their works exploited the concept in formulating some expressions needed for the solutions of the diffusion equations due to longitudinal development in the EM cascade theory. It was then applied to the lateral spread of electrons around the cascade axis while solving the diffusion equations in the three-dimensional EM cascade theory.

The most simple and earliest description of the EM cascade was being started with the longitudinal development. One of the most popular analytic representations of the average longitudinal profile was provided by Greisen [3]. This so called Greisen profile was obtained from the calculations carried out by Snyder in the so called approximation B (taking into account only three processes, (a) pair production by the photons, (b) *bremsstrahlung* by the electrons and, (c) collision energy loss suffered by the electrons), is given by

$$N_{\rm e} \;=\; \frac{0.31}{\sqrt{\ln(E_0/\epsilon_0)}}\;\exp[X(1-1.5\;\ln(s_{\|})], \tag{3.1}$$

where $s_{\|}$ gives the stage of the longitudinal cascade development, E_0 is the energy of the primary photon generating the cascade (the atmospheric depth X is expressed in cascade units; it is normalized by the radiation length of electrons in air, that is equal to 37.1 g cm^{-2}).

The average evolving stage of pure EM cascades is expressed primarily by the longitudinal shape or $s_{\|}$ parameter. It is essentially the inverse of the fractional rate of change of the total electron number of an EAS with atmospheric depth

[1]. This fractional rate of change is called the size slope $\lambda(s_{\parallel})$ as

$$\lambda(s_{\parallel}) = \frac{1}{N_{\rm e}(X)} \frac{{\rm d}N_{\rm e}(X)}{{\rm d}X}. \tag{3.2}$$

Thus, the shower age is simply related to the rate of growth and decay of $N_{\rm e}(X)$ in a shower, and mathematically expressed by the operation $\lambda^{-1}(\frac{1}{N_{\rm e}(X)} \frac{{\rm d}N_{\rm e}(X)}{{\rm d}X})$.

After doing a few mathematical operations to the equation 3.2, Rossi and Greisen attributed a more direct physical meaning to the shower age as a shape or spectral index of the energy spectra of EM particles. In a shower initiated by an electron or photon, the energy spectra of secondary electrons or photons follow a power law of the form,

$$n_{\rm e/\gamma}(E) \sim E^{-(s+1)}. \tag{3.3}$$

The power law works above the critical energy ϵ_0, where ϵ_0 is the energy value at which ionization and *bremsstrahlung* energy losses are equal, by an electron, which happens at $\epsilon_0 \approx 82$ MeV for electrons in air.

After the preliminary work of Moliére and Bethe, focusing on the lateral electron distribution near the cascade maximum, Nishimura and Kamata described the lateral development under the assumption that electrons suffer constant amount (energy independent) of collision loss per radiation length, which is equal to the critical energy (approximation B) [4] by solving the 3D diffusion equations. Fitting their numerical results on the electron densities, Nishimura and Kamata were able to propose a first r-dependence analytic expression for the shower age $s_{\parallel}$

$$s_{\parallel} = \frac{3X}{X + 2\ln(E/\epsilon_0) + 2\ln(r/r_{\rm m})}, \tag{3.4}$$

where X is the atmospheric slant depth (in electron radiation length unit) of the observational level, E is the energy of the primary electron/gamma; r and $r_{\rm m}$ are the radial distance from the shower core, and the Moliére radius ($r_{\rm m}$ corresponds the radius of a cylindrical region where $\sim 90\%$ of the EM shower energy is deposited, that is, $r_{\rm m} \sim 80$ m at sea level). With this definition, $s_{\parallel} = 0$ at the top of the atmosphere and $s_{\parallel} \sim 1$ at the depth of shower maximum. Under the same theoretical framework, the LDF of cascade particles advancing through a constant air medium, was expressed approximately by Greisen, and is very well-known as

the (NKG) structure function [3], given by

$$\mathrm{f}(r) = \mathrm{C}(s_\perp)(r/r_\mathrm{m})^{s_\perp-2}(1+r/r_\mathrm{m})^{s_\perp-4.5} \ , \tag{3.5}$$

where $s_\perp$ essentially describes the slope of the LDF which is determined from the shape of the observed lateral distribution of electrons in an EAS. The normalization factor $\mathrm{C}(s_\perp)$ in the equation 3.5 is given by

$$\mathrm{C}(s_\perp) = \frac{\Gamma(4.5-s_\perp)}{2\pi\Gamma(s_\perp)\Gamma(4.5-2s_\perp)} \ . \tag{3.6}$$

An expression for the electron density (ρ_e) in terms of the profile function $\mathrm{f}(r)$ (thanks to the properties of the Eulerian function as shown in Appendix: A.1.3) is,

$$\rho_\mathrm{e}(r) = \frac{N_\mathrm{e}}{r_\mathrm{m}^2}\mathrm{f}(r) \ . \tag{3.7}$$

The relation $s_\parallel = s_\perp$ holds for EM showers [4]. Such equivalence implies the correlation between steeper lateral distributions ($s_\parallel < 1$) or flatter lateral distributions ($s_\parallel > 1$) in proportion to the distance to shower maximum. It suggests also the employment of the parameter $s_\perp$ as a hint of the global shower cascading expected to depend on shower initiating particle and several interaction features (cross-section, multiplicity and in-elasticity).

However, Nishimura, Kamata and Greisen noted some difficulties when comparing the prediction of the cascade theory with the measured lateral distributions of electrons in EAS. We have listed hereunder some limitations on the validity of the analytical expressions caused by the various approximations (so-called approximations A and B) in obtaining the solutions as well as due to over-simplification of the adopted 3D transport equations. The validity of the equation 3.5 therefore obeys some conditions, which are as follows:

- $E_0/\epsilon_0 \gg 1$; due to the asymptotic value of the cross sections
- $X > 1$; more than one radiation length unit is necessary to consider the continuity in the cascade
- $\mid \log(E_0/\epsilon_0) \mid \gg \mid \log(r/r_\mathrm{m}) \mid$

The last condition may be not satisfied in the vicinity of the EAS axis as underlined by Nishimura considering not appropriate to use the formula near the EAS core. Nishimura and Kamata also ascertained that corrections were necessary to their calculations performed for the homogeneous medium. In consequence, taking into account the variation of the air density, they inferred that in order to compare the theoretical curves with the experimental data, the distribution obtained at about 2 radiation length (with approximation B) above the measurement depth must be used.

Solutions of the 3D diffusion equations came from simultaneous operations such as solutions of adjoining equations, the Bessel Fourier transformation being applied to r, the numerical integration on X, and on the energy E being performed by partial polynomial functions [5, 6]. This method, which involves several approximate steps and numerical inverse transformations, leads undoubtedly to a limiting (as $E_0 \rightarrow \infty$) lateral distribution of EAS electrons, e.g. the NKG LDF. The meaning of *limiting* actually refers to the energy condition i.e., E_0 or $E >> \epsilon_0$ through the saddle point solutions in approximation A, and the negligible collision losses of electrons in approximation B, that have been used to obtain the NKG LDF.

The equation 3.1 concerns the total number of electrons of the cascade, whereas a parallel relation for the integral energy spectrum of the electrons is also given; in both cases cross sections for *bremsstrahlung* and pair production in their respective asymptotic form at very high energy have been exploited. In this useful synthesis the $s_{\|}$ parameter is defined simply as

$$s_{\|} = \frac{3X}{X + 2X_{\max}}. \tag{3.8}$$

So far the concept of the shower age is elaborated explicitly from the angle of purely EM cascade theory. An extension of the concept is applied also to hadron initiated showers. It was Cocconi who first pointed out that the equations 3.1, 3.5 and 3.8 provide a complete procedure for calculating the lateral development of a pure EM cascade [7]. A hadronic shower is not a pure EM cascade but consists of a superposition of many pure independent EM cascades that usually build the lateral distribution of electrons of the shower. Hence, a resulting single cascade with a modified shape parameter will effectively describe both the longitudinal

and lateral structures of electrons for the hadron initiated shower [4]. This is a possible reason why the analytical expressions in 3.1, 3.5 and 3.8 from the EM theory are only rough approximations for the description of hadron initiated showers.

In some earlier analyses of observed EAS data, it was found that electron densities at large core distances were noted to be larger than NKG predicted values [8, 9]. The muon decay process might be a possible reason for the origin of it. On the other hand, the original NK (Nishimura-Kamata) predicted electron densities near the core were found a little higher than those with the NKG in the domain $s \geq 1.2$ [10]. It was also noted in MC simulations that the NKG formula was quite useful for proton initiated showers and is much faster than the full simulation of the EGS cascade [11].

In EAS studies a significant part of various discrepancies among theory, simulation and experiment is of course due to the application of a pure EM cascade (NKG type LDF) to hadronic showers. But, discrepancies might also come either from the simplistic treatment of scattering processes (e.g. the multiple coulomb scattering and also Bhaba, and Moller scattering) in NKG or neglecting of effects like photo-production, geomagnetic deflection. Also hadronic interactions affect the shape of the lateral distribution of electrons to some extend.

The limitations of various instruments used in an EAS experiment may also sometimes give rise to discrepancy. For example, while detecting large showers in KASCADE experiment (suppose, the setup is appropriate to observe medium size showers), the detectors close to the EAS core get saturated and should not be considered for the analysis. Then, the LDF does not provide a better fit for large showers at smaller distances and for small showers at larger distances [12].

Many authors therefore replace the NKG type LDF with slightly different functions [13], or modify the LDF by changing the parameters of the exponents to account for the hadronic origin of showers in EAS data. The second treatment was indeed implemented by the KASCADE-Grande collaboration to provide a better agreement to the shape of the observed lateral distribution of electrons with the corrected NKG function [12].

In Tien Shah experiment, a steeper profile was exhibited near the core by electron density data, and it was suggested that the NKG LDF be corrected by replacing the Moliére radius r_0 with $0.6\mathrm{r}_0$ for a better agreement [14].

The MC calculations of Hillas [15] were used to improve the NKG LDF by simultaneous modifications of the exponents and the Moliére unit to achieve better agreement with data. It was suggested by some authors that variation in the Moliére unit, instead of the exponents, will lead to a better improvement for the fit behaviour of the NKG function. This was subsequently implemented to the NKG function by Uchaikin and later the KASCADE group by replacing the Moliére radius with a longitudinal age dependent effective Moliére radius [5, 6, 16]. The Uchaikin LDF has restricted applicability, it does not work well to fit individual shower owing to large fluctuations between the detector locations. This modified NKG LDF was actually implemented in the so called NKG subroutine of CORSIKA for the analytical treatment of EM component in a shower.

A theoretical prediction was made by Capdevielle with regard to the errors introduced by the NKG function in shape and shower size determination [17]. It was then supported by many observations (e.g. in [18]), and subsequently concluded by Capdevielle et al. [17, 19] that the NKG function with a single age cannot describe the lateral distribution of electrons. Consequently, the notion of *local age* emerged [11, 17].

Attempts were made by several EAS experiments [5, 6, 12–15] to assign important physical significance to the parameter $s_{\perp}$, that is obtained from the fit on the observed density data of electrons, as predicted by the EM cascade theory. Some experiments such as GRAPES-3 [20], ARGO-YBJ [21] etc. have realized that it could be a potential observable to study the PCRs. In the cascade theory, the parameter is supposed to relate with the stage of development of EAS in the atmosphere [4]. Distribution of secondary electrons either in spatial or energy space on the ground depends only on the stage of longitudinal shower development in the atmosphere or equivalently on $s_{\parallel}$. An equality between these two shower age parameters exists in the cascade theory for pure EM showers. However, such equality is also maintained approximately by hadron induced showers [4, 22].

Recent studies indicate that the average shape of a number of distributions of electrons in showers initiated by hadrons exhibit the so called *universality* [23–28]. The fact that the *universality* property of air showers [29, 30] is such a powerful tool for the analysis of EAS data can also be understood from the essence of the concept of shower age. According to the *universality* property, all showers follow a similar development in the vicinity of their shower maxima, where they also share the same shower age. These showers, for an equal density profile of the medium also have the same lateral spread around the cascade axis.

It was also demonstrated [4, 22] that for hadron initiated EAS, the longitudinal and lateral profiles of the EM component can be described by some average overall single cascade, assigning a suitable value to the age parameter. The so-called universality property of simulated showers has been established for EAS induced by primaries at ultra-high energies in terms of the shape parameter $s_{\parallel}$ [23, 24, 26] using $X_{\max}$. However, observed lateral density distribution of electrons is usually described in terms of $s_{\perp}$ and in most experiments the estimated lateral/transverse shower age i.e. the $s_{\perp}$ differs from the $s_{\parallel}$ for EAS with hadrons as primaries. It was suggested from the experimental results [14, 31] that these two age parameters are connected through the (approximate) relation $s_{\parallel} \geq s_{\perp} + \delta$, with $\delta \approx 0.2$. Some early MC simulation results obtained a relation of the nature $s_{\parallel} \sim 1.3 s_{\perp}$ [32]. The $s_{\parallel}$ parameter can be estimated observationally only if EAS experiments are equipped with Cherenkov or fluorescence detectors, whereas the $s_{\perp}$ parameter follows straightway from the LDF for electrons which is the basic measurement of any conventional EAS array consisting of particle/scintillation detectors.

In this chapter, a correlation between $s_{\perp}$ and the stage of the longitudinal development will be examined using simulated EAS data according to the prediction from the EM cascade theory. Next, we investigate various characteristic features of the parameter and its relationship with some other important EAS parameters using MC simulations. In this context, we have to consider some observed results from two sea level experiments i.e. NBU and KASCADE for the purpose of comparison and interpretation. The NBU air shower array is located at North Bengal University campus, India (latitude $26^{o}42'$ N, longitude $88^{o}21'$ E, 150 m a.s.l., area 2000 m^2), was being operated during 1980 - 98 [33]. The KASCADE experiment is located at Forschungszentrum Karlsruhe, Germany (latitude 49.1^{o}

N, longitude 8.4^{o} E, 110 m a.s.l., area 40000 m^2) [34]. Our main objective is to explore the significant contribution of $s_{\perp}$ in a so-called multi-parameter approach of studying EAS data to derive possible conclusions on the nature of shower initiating particles around the *knee* region.

We have used the original form of the NKG LDF to fit the density of electrons whereas in the KASCADE work the modified form of the NKG was used [12]. Moreover, in their work, two secondary estimators were used for the measurement of energy and mass. The nature of variation of the shape parameter was studied as a function of these estimators independently. In the present work, we show that the slope of the LDF of EAS electron distribution from a detailed MC simulation study indicates the stage of development of showers in terms of $s_{\perp}$. We also investigate the fluctuations in $s_{\perp}$ arising from its frequency distributions and the correlation of the fluctuation parameter with $N_{\rm e}$ for proton and iron showers. An important correlation of $s_{\perp}$ simultaneously with $N_{\rm e}$ and $N_{\mu}^{\rm tr.}$ ($N_{\mu}^{\rm tr.}$ takes into account the total number of muons from a defined radial bin, e.g. 4–35 m at NBU level) are studied in a so called multi-parameter approach. Efforts are also made to explore whether the $s_{\perp}$ has any correlation with the $s_{\parallel}$ parameter. It is expected that a more direct application of these parameters from the original LDF or Greisen profile function to simulated or observed data will provide an opportunity to re-examine the important predictions in the EM cascade theory better. For generating MC shower events, the air shower simulation program CORSIKA version 6.970 [35] has been used in the work.

3.3 Simulation and data analysis

The hadronic interaction model QGSJet01.c [36] is considered for interaction processes above $80\mathrm{GeV/n}$ energy. The model is combined with the low energy hadronic model GHEISHA version 2002d [37] that works below $80\mathrm{GeV/n}$. All these models are embedded in the CORSIKA MC program version 6.970 [35]. Although the low energy interaction model GHEISHA has some shortcomings but it does not have significant effect on the secondary particle distribution except at very large core distances [38]. For the EM part the EGS4 [39] program package has been embedded in the Monte Carlo code for carrying out interactions in the EM component. The high-energy hadronic model SIBYLL version

2.1 [40] is considered to check the potential impact, of the high-energy hadronic models on some of our important findings.

In the CORSIKA MC code, the US-standard atmospheric model [41, 42] with planar approximation is used for the generation of EAS events with zenith angles $\Theta < 70^{\rm o}$. We have simulated events with Θ that ranges between $0^{\rm o}$ and $50^{\rm o}$. The EAS events have been generated for proton, helium and iron nuclei as primaries in the primary energy interval of 10^{14} eV to 3×10^{16} eV with about 20000 events for each primary. The spectral index of the primary energy spectrum has been taken as -2.7 up to the *knee* (3×10^{15} eV) and as -3.1 beyond the *knee* in the simulation. A mixed composition sample has also been prepared from the generated showers containing 50% proton, 25% helium and 25% iron showers. The simulated showers have been generated at the altitude and geomagnetic fields corresponding to the North Bengal University air shower array. At the ground plane the kinetic energy cut-offs are set at 50 MeV and 3 MeV for muons and electrons. A smaller sample of simulated events has also been generated for KASCADE conditions to observe the nature of variation of the $s_{\perp}$ with other observables. The kinetic energy cut-offs are set at 230 MeV and 3 MeV for muons and electrons for KASCADE [12].

The simulated densities for electrons at different radial distances from the EAS core are used for shower fit, employing the NKG type LDF for obtaining $s_{\perp}$ parameter. It should be however mentioned that other EAS parameters such as $N_{\rm e}$, N_{μ}, Θ and Φ are used directly from the generated events. Only the $s_{\perp}$ parameter is obtained from the fit using simulated/observed data. The KASCADE data for $\rho_{\rm e}$ are obtained from published papers corresponding to different $N_{\rm e}$ bins [16].

In order to check the effectiveness of the NKG LDF in describing the simulated density of electrons, we have applied the fit procedure to the simulated density data. The estimation of the $s_{\perp}$ parameter is performed by means of a chi-square minimization routine using gradient search technique. In this procedure the simulated electron densities in the radial interval $7 - 102$ m are compared with the NKG LDF. It is found that the NKG function represents the simulated data satisfactorily over the whole radial distance except at very small distances, where the simulated densities are found a little higher than that given by the NKG function. Hence, the simulated densities only in the radial interval $7 - 102$ m are used, and

fitted showers with reduced χ^2 less than 4 are only accepted for results. For primary energies around 10^{14} eV, the extension of a shower is usually spread over within $\sim$ 40 m core distance whereas it exceeds $\sim$ 100 m for energies around the *knee*. In the Fig. 3.1, we have plotted the simulated electron densities over the range $7 - 102$ m for a particular N_e obtained with the QGSJet model and its comparison with the NKG fitted curve.

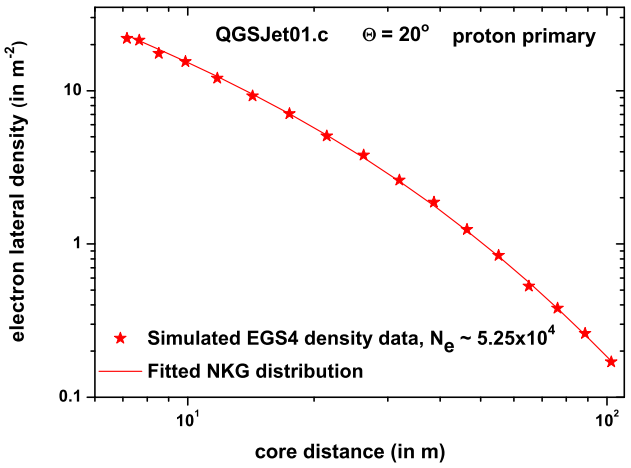

FIGURE 3.1: Comparison of the NKG fitted lateral distribution of electrons with the simulated data for showers generated at 5×10^{14} eV energy.

The errors of the $s_\perp$ estimation in the interval, N_e : 10^3–10^5 are obtained as ± 0.034 for the QGSJet01.c and ± 0.052 for SIBYLL v.2.1. The SIBYLL model shows relatively higher uncertainty of the $s_\perp$ estimation and that might have originated from comparatively a smaller sample size of simulated data in this case.

3.4 Results and discussions

3.4.1 Dependence of lateral shower age on atmospheric depth

With the increase of Θ, a shower traverses an increased thickness of atmosphere which immediately suggests that the EAS with higher Θ should be older in shower age than the EAS of smaller Θ but of same primary energy. Based on this idea, we have studied variation of $s_\perp$ with atmospheric depth from the simulated data.

Figs. 3.2a, 3.2b and 3.2c show the $s_{\perp}$ as a function of atmospheric depth for three different intervals of shower size, $(1.8\text{–}3)\times10^3$, $(5.7\text{–}9.5)\times10^3$ and $(2.0\text{–}5.0)\times10^4$, obtained from MC simulations. Separate samples of proton and iron initiated showers are considered to investigate the mass dependence. Besides, we have used our prepared mixed composition sample as described in the section 3.3 for this study as well. In the Fig. 3.2c, we have included the NBU data [43].

It can be seen from the figures that for both proton and iron initiated showers, $s_{\perp}$ monotonically increases with atmospheric depth reflecting a strong correlation of the parameter with longitudinal development. The nature of $s_{\perp}$ versus atmospheric depth ($\sec\Theta$) variation does not have any noticeable dependence on shower size in the considered shower size range.

For mixed primaries the $s_{\perp}$ parameter is found to vary relatively slowly with atmospheric depth and even noticed to remain nearly constant at some $N_{\rm e}$ intervals (see Fig. 3.2a). This is due to the fact that showers initiated by heavier primaries dominate in the mixed composition sample when $\sec\Theta$ values are small. But, showers initiated by lighter primaries contribute most in the mixed sample for larger values of Θ in the same $N_{\rm e}$ interval. Similar explanation is valid also to the observed variation in the Fig 3.2c. However, NBU data show relatively higher values for $s_{\perp}$ in comparison with mixed data. Such a behavior from observation is obvious, because the observed shower events may contain species other than $\mathrm{Z} = 1, 2, 26$. Contamination of species with $Z > 2$ in NBU data might possibly push the $s_{\perp}$ versus $\sec\Theta$ curve close to the simulated iron curve.

The present simulation study suggests that the $s_{\perp}$ parameter can be expressed as a function of Θ by the empirical relation

$$s_{\perp} = s_{\rm o} + \mathrm{A}\ sec\ \Theta. \tag{3.9}$$

The values of s_0 and A for different $N_{\rm e}$ ranges obtained by fitting the simulated data generated with the QGSJet model are shown in Table 3.1.

Equation 3.9 can be written as $s_{\perp} = s_{\rm o} + \mathrm{A}\ \frac{X}{X_{\rm v}}$, where X and $X_{\rm v}$ are the atmospheric thickness traversed by the EAS and the vertical atmospheric depth respectively. It thus immediately follows $\frac{{\rm d}s_{\perp}}{{\rm d}X} = \frac{\mathrm{A}}{X_{\rm v}}$. The change of $s_{\perp}$ over an atmospheric depth of ~ 100 g cm^{-2} for the simulations (mixed) generated with the

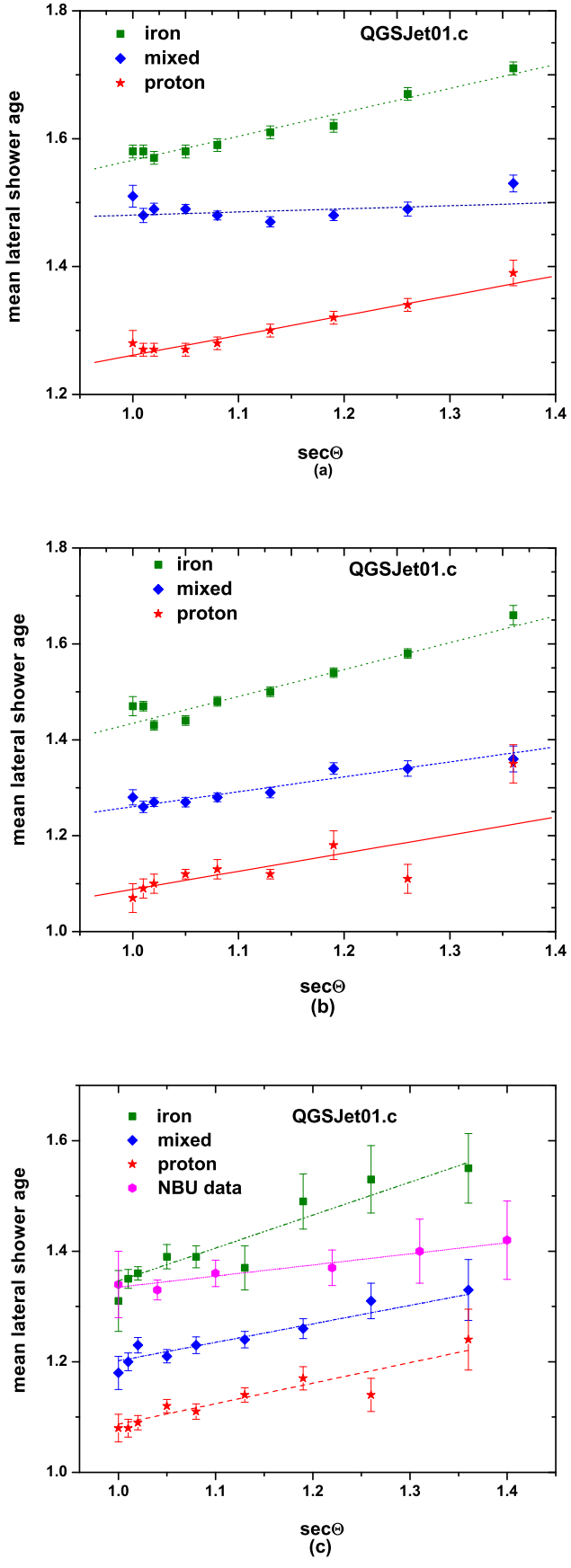

FIGURE 3.2: Variation of shower age parameter ($s_\perp$) with atmospheric slant depth ($\sec\Theta$) for three N_e ranges: (a) $(1.8–3.0)\times10^3$; (b) $(5.7–9.5)\times10^3$ and (c) $(2.0–5.0)\times10^4$ at NBU level. In (c) NBU data are provided.

TABLE 3.1: Parameters from the variation of $s_\perp$ with $\sec\Theta$ for three different N_e intervals. The NBU data are shown for one N_e interval only.

$N_e \times 10^3$		$1.8-3.0$	$5.7-9.5$	$20-50$
proton	s_o	$0.95 \pm .03$	$0.71 \pm .15$	$0.71 \pm .09$
	A	$0.31 \pm .02$	$0.37 \pm .14$	$0.37 \pm .08$
iron	s_o	$1.19 \pm .03$	$0.87 \pm .07$	$0.74 \pm .13$
	A	$0.37 \pm .03$	$0.50 \pm .08$	$0.59 \pm .12$
mixed	s_o	$1.43 \pm .05$	$0.95 \pm .05$	$0.87 \pm .08$
	A	$0.04 \pm .04$	$0.31 \pm .04$	$0.33 \pm .07$
NBU data	s_o	–	–	1.13 ± 0.04
	A	–	–	0.20 ± 0.03

QGSJet model are $\frac{A}{X_v} \times 100 = \frac{0.31}{1000} \times 100 \sim 0.031$ and ~ 0.033 for two N_e ranges such as $(5.7–9.5) \times 10^3$ and $(2.0–5.0) \times 10^4$ respectively. At mountain altitude, the Mount Norikura group also reported similar results [44].

In order to check the influence of the hadronic interaction models on the results obtained, we compare $s_\perp$ versus $\sec\Theta$ variations for two different models, QGSJet and SIBYLL, which are shown in the Fig. 3.3. The SIBYLL yields comparatively a higher value for $s_\perp$ than QGSJet but the nature of dependence of the $s_\perp$ parameter on atmospheric depth is found similar in both the hadronic models. The discrepancy may come from the cross-section for proton-air collisions that rises more rapidly versus energy in SYBILL than in QGSJet.

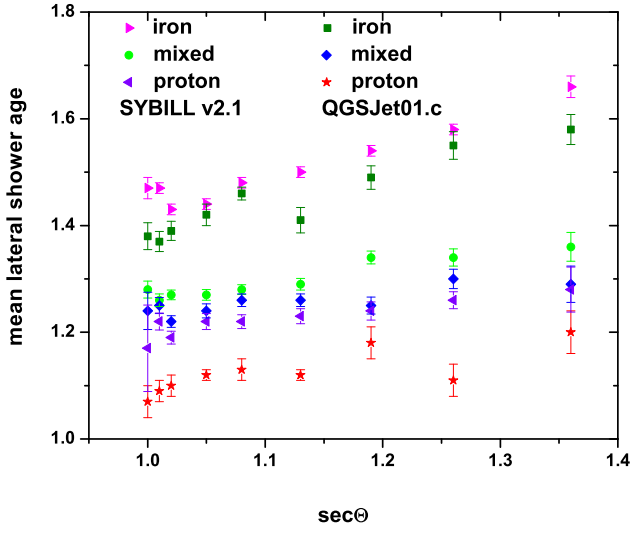

FIGURE 3.3: Variation of $s_\perp$ with $\sec\Theta$ for two different interaction models, QGSJet and SIBYLL corresponding to the N_e interval $(1.8–3.0) \times 10^3$ at NBU level.

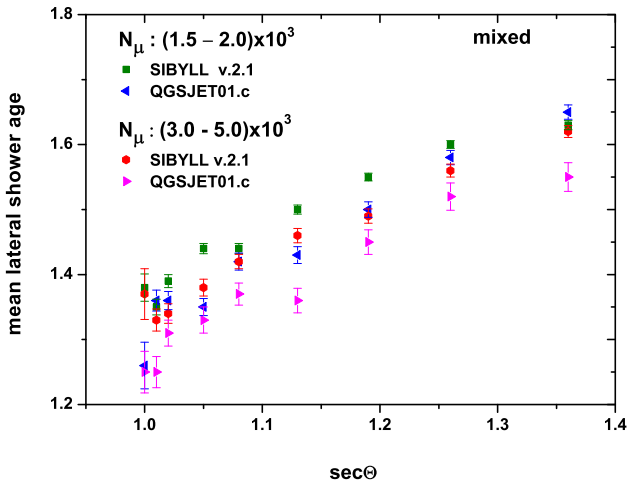

FIGURE 3.4: Variation of $s_\perp$ with $\sec\Theta$ for two muon size intervals using two high-energy hadronic interaction models at NBU level.

The variation of $s_\perp$ with $\sec\Theta$ is also studied for two different N_μ bins, which are shown in the Fig. 3.4. We have included possible effects arising from the employment of different high-energy hadronic models into the results. As found in the Fig. 3.3, the SYBILL still maintains a little higher value for $s_\perp$ relative to the QGSJet.

3.4.2 Correlation between $s_\parallel$ and $s_\perp$

In MC simulations the development of EM cascades towards the ground is calculated with the EGS4 code. The $s_\parallel$ parameter in terms of the numerical values obtained from the EGS4 simulation code attributes a more refined procedure than what obtained from the EM cascade theory. Capdevielle et al. implemented an approximate formula for the $s_\parallel$ parameter for the EGS4 code [45, 46]:

$$s_\parallel = \exp\left[0.67 \times \left\{1 + \frac{\alpha}{X} - \tau\right\}\right], \tag{3.10}$$

where $N_{\max}$ is the shower size corresponding to $X_{\max}$ of a shower and $\alpha = \ln\frac{N_{\max}}{N_e}$, and $\tau = \frac{X_{\max}}{X}$. The output data file is used to obtain the $s_\parallel$ parameter employing the equation 3.10. Such $s_\parallel$ parameter is used for comparison [45, 46] with the predicted value by the cascade theory in approximation B.

Hence, the shower age $s_\parallel$ can be estimated knowing both $N_{\max}$ and $X_{\max}$. The difference between the two age parameters, $s_\parallel$ and $s_\perp$, is studied. A frequency

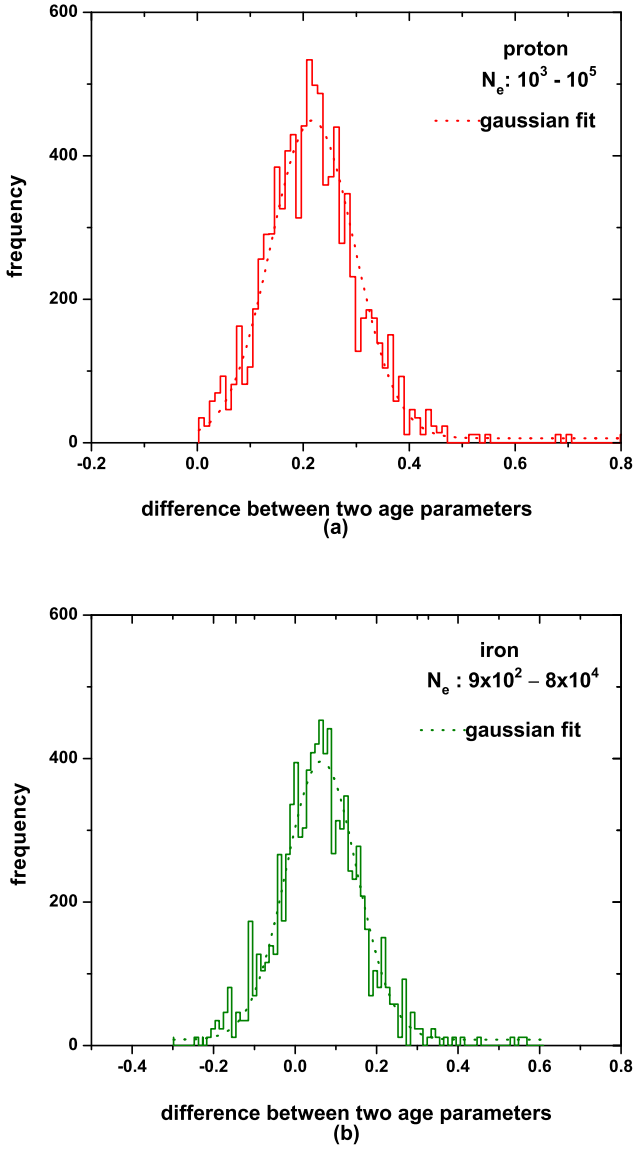

FIGURE 3.5: Distributions of differences between $s_{\parallel}$ and $s_{\perp}$ at NBU level.

distribution of differences between two age parameters is given in the Fig. 3.5a for proton induced showers. It is revealed from the figure that the frequency distribution peaks around $0.22 \pm .002$ which is consistent with the early observations [26]. But, for iron showers the peak in the distribution occurs around a relatively lower value of $0.06 \pm .003$, and is shown in the Fig. 3.5b.

3.4.3 Distribution of $s_{\perp}$

The distributions of $s_{\perp}$ are obtained from fitted showers for the primary energy range 3×10^{14}–3×10^{16} eV and are shown in Figs. 3.6a and 3.6b. A Gaussian

distribution function does not nicely fit these distributions. Deviations from the Gaussian nature become visible or distributions become asymmetric when the observational level is much deeper than the depth of the shower maximum, which is the case for both KASCADE and NBU levels. In those cases, fitting quality can be improved by an Extreme Value Distribution (E.V.D.) function. The E.V.D. probability density function for the $s_\perp$ parameter has the following form,

$$f_{\rm EVD}(s_\perp) = \frac{1}{\sigma_{s_\perp}} \exp\left[\pm\frac{(\mu - s_\perp)}{\sigma_{s_\perp}} - \exp\left\{\pm\frac{(\mu - s_\perp)}{\sigma_{s_\perp}}\right\}\right]. \tag{3.11}$$

The parameters μ and $\sigma_{s_\perp}$ are related to the average size $\overline{s_\perp}$ and its variance $\mathrm{V}_{s_\perp}$ by $\overline{s_\perp} = \mu \pm 0.577\ \sigma_{s_\perp}$ and $\mathrm{V}_{s_\perp} = 1.645{\sigma_{s_\perp}}^2$. In Figs. 3.6a and 3.6b, we have shown histograms for $s_\perp$ obtained from our MC simulations. In these figures, the frequencies reflect the intensities of primaries around the *knee*. The long tail in the left wing of Fig. 3.6a for example corresponds to very penetrating proton showers of low primary energy and conversely the steep right wing contains showers interacting at very high altitude whereas the central part is populated by showers with an individual maximum close from average maximum at each energy. Similar features concerning the case of pure iron component (Fig. 3.6b) with a general reduction in $\sigma_{s_\perp}$ value of the fluctuation. As an example, the analysis of the Fig. 3.6b by the E.V.D. yields $\sigma_{s_\perp} = 0.07$ and $\mu = 1.495$. From the Fig. 3.6a, we will obviously obtain different set of values for these parameters. Hence, it reveals that these frequency distributions fitted by the E.V.D., could be useful for extracting information on EAS initiated primaries around the *knee*.

In the Fig. 3.7a, a small N_μ range is considered in order to distinguish between frequency distributions of $s_\perp$ for proton and iron induced showers at the NBU level. This study could be very effective to extract information on the mass composition of PCRs in data at sea levels. We describe the typical histograms here by the E.V.D. function also.

Frequency distributions of $s_\perp$ for proton and iron showers in the same N_μ range like Fig. 3.7a are presented through the Fig. 3.7b at a high altitude location in order to correlate the $s_\perp$ with longitudinal development of an EAS (here, we have used our analyzed simulated data from the work in [47]). As the mountain level is not much deeper than the depth of the shower maximum, the asymmetries of the $s_\perp$ distributions will be marginal and can be conveniently described by the

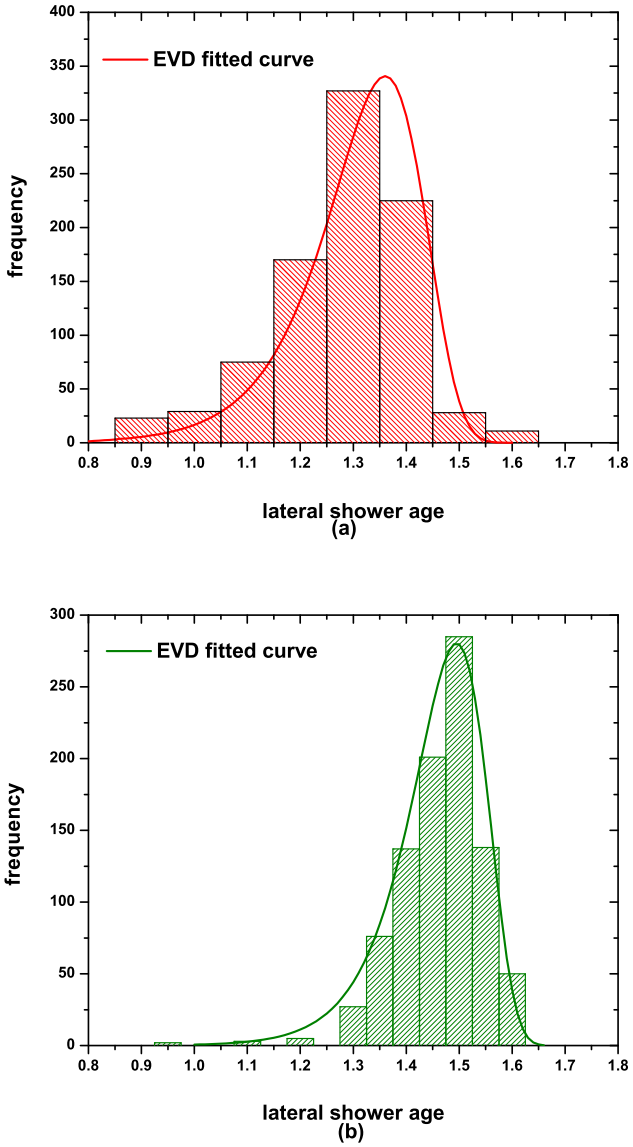

FIGURE 3.6: Distributions of $s_\perp$ for vertically incident showers at the NBU level for the energy range $E = 3 \times 10^{14}$–3×10^{16} with the QGSJet model; (a) proton and (b) iron. Fits are made by the EVD function. For (a) $\mu \approx 1.38$ and $\sigma_{s_\perp} \approx 0.1$ and (b) $\mu \approx 1.495$ and $\sigma_{s_\perp} \approx 0.07$.

Gaussian distribution function. Therefore, the $s_\perp$ histograms in the Fig. 3.7b are fitted by the Gaussian distribution function. Distributions in the Fig. 3.7b suggest that the smaller $s_\perp$ values account for the smaller extents of EAS longitudinal developments and showers are regarded as young. Comparison of mean values either for proton or iron initiated showers between the Figs. 3.7a and 3.7b speak for themselves. This is in agreement with the prediction from the EM cascade theory. The EM theory argues that the LDF shape parameter will not differ much from its value at $X_{\max}$ for altitudes relatively nearer to $X_{\max}$ and the condition

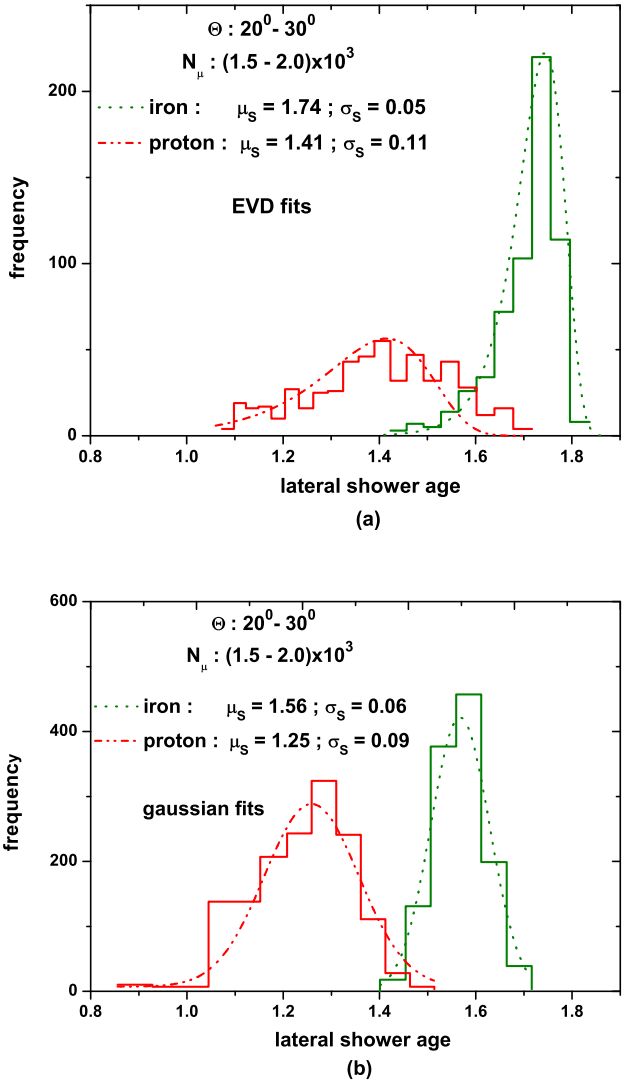

FIGURE 3.7: In (a) the distributions of $s_\perp$ are shown for proton and iron showers at the NBU level (sea level) with EVD fits. In (b) the distributions are shown at ARGO-YBJ level (mountain level) with Gaussian fits. The QGSJet model is used entirely.

$s_\perp \approx s_\parallel \approx 1$ is also valid.

The fluctuations in $s_\perp$ are larger for proton initiated showers in compared to those initiated by heavier primary as revealed from all the figures in Figs. 3.6 and 3.7 .

3.4.4 The fluctuation of $s_\perp$ as a function of shower size

The fluctuations of $s_\perp$ in different smaller shower age bins are estimated and plotted with increasing mean N_e for proton and iron showers in the Fig. 3.8.

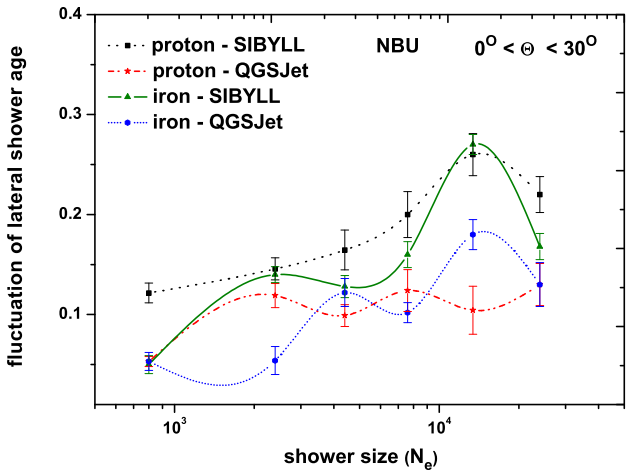

FIGURE 3.8: Fluctuations in $s_\perp$ and their variation with N_e at the NBU level.The lines are only a guide for the eye.

It is found that fluctuations in $s_\perp$ are larger for EASs induced by proton than iron, except at lower energies. This is in accordance with the predictions made in [48]. However, the SIBYLL introduces little higher fluctuations to $s_\perp$ in compare to fluctuations contributed by the QGSJet model for any particular type of primary. It appears from the Fig. 3.8 that fluctuation (i.e. the R.M.S of variance of $s_\perp$) has essentially zero mass-separation power but rather a quite large model-dependence.

3.4.5 Variation of $s_\perp$ simultaneously with N_e and N_μ: A multi-parameter approach

Muon content of EAS is generally used to extract information on the composition of CR primaries. However, due to uncertainties in the interaction model and the difficulties associated with the solutions to the EAS inverse problem, separating the primary energy spectra of elemental groups remains ambiguous. Proton and iron initiated showers may be better separated employing $s_\perp$ and N_μ simultaneously through 3-dimensional plot of N_e versus N_μ and $s_\perp$ than in either of its 1-dimensional projections. It is found that accuracy of determining the nature of primary species increases with the simultaneous use of $s_\perp$ and N_μ against N_e or E. In Figs. 3.9a, 3.9b, 3.10a and 3.10b, we plot the 3-dimensional curve between $\overline{s_\perp}$, $\overline{N_\mathrm{e}}$ and $\overline{N_\mu}$ obtained from the simulations for both proton and iron primaries

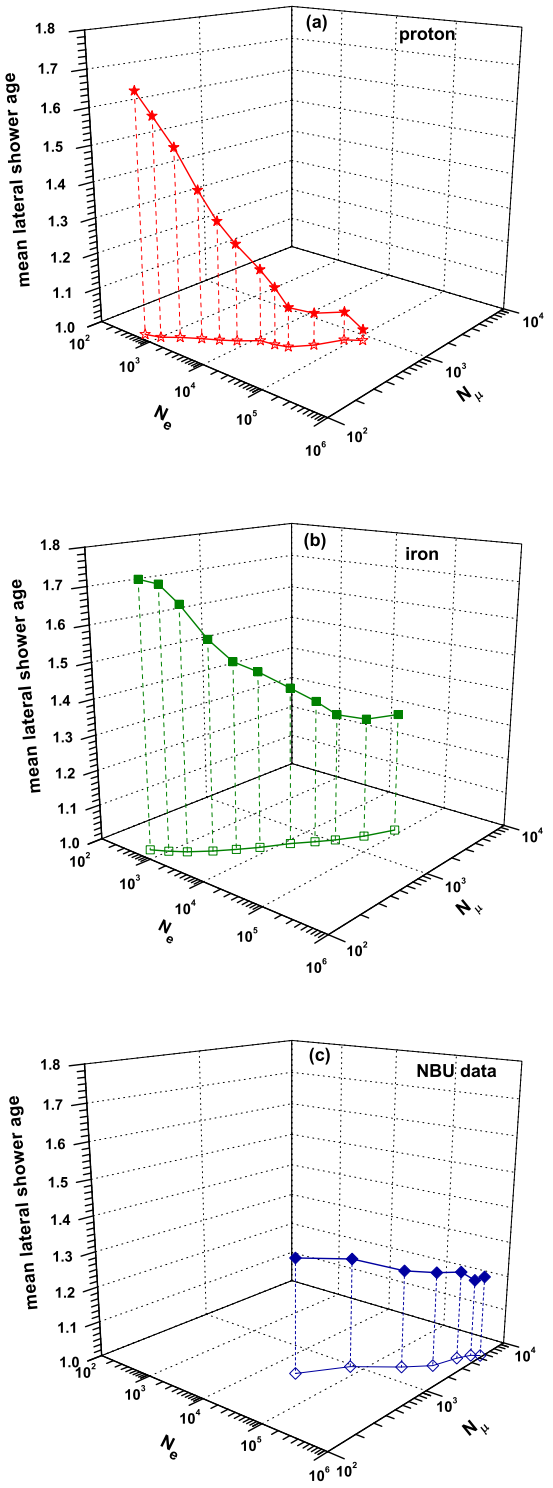

FIGURE 3.9: 3-Dimensional plot using shower size, muon size and lateral shower age parameters at NBU level: (a) Pure proton and (b) Pure iron showers, generated using the QGSJet model. NBU data are given in (c). Muons are considered from 4–35 m core distance with $E_\mu^{\mathrm{Th.}} \geq 2.5$ GeV. Projection on the X–Y plane showing the corresponding N_e–N_μ curve.

at NBU and KASCADE levels. The corresponding observational results of the two experiments are also shown through the Figs. 3.9c and 3.10c.

For the NBU data, measurements of various observables are made over a limited energy window [33]. The detecting efficiency of the NBU array within its detecting area is greater than 90% for showers of size range $\sim 10^4$ to 10^6. The array achieves $\sim 1.1^{\rm o}$ angular resolution in the Θ range $0^{\rm o} - 40^{\rm o}$. However at higher zenith angles ($> 40^{\rm o}$), the resolution becomes increasingly poorer, it becomes $4^{\rm o}$ around $55^{\rm o}$ zenith. The energy resolution corresponds to shower size resolution in the NBU experiment. The accuracy of the size estimation depends on fluctuations in the cascade development in the atmosphere. Fluctuations of size are studied employing MC simulation. Fluctuation of size estimation increases with the decrease of angular resolution i.e. with increasing zenith.

The muon detecting system could detect and measure muons associated with an EAS up to a momentum 500 GeV/c. The lower cutoff energy of muons, provided by the lead and concrete absorbers placed above the pair of magnet spectrograph is 2.5 GeV. The measurement for the N_μ are made considering muon density data within a limited radial distance range of 4–35 m only. To get better comparison between simulation and experiment in NBU, we have sorted out muons from the region of $r = 4$–35 m range with momenta $p_\mu \geq 2.5$ GeV/c from generated events. A comparison among three figures in 3.9a, 3.9b and 3.9c indicates that the NBU data though obtained in a small energy window but still hint for a mixed composition across the *knee*. The result shows that the 3-dimensional plot is more distinct although we have constraints on the NBU muon data for the PCR composition study than its 2-dimensional projection through the $N_{\rm e}$–N_μ curve.

In the case of KASCADE data, we have estimated $s_\perp$ from their measured lateral distribution [43, 49, 50] employing our fit procedure for a given $N_{\rm e}$ bin. The corresponding N_μ are extracted from the N_e–N_μ curve [51]. The comparison of simulated results with data from the KASCADE experiment on the basis of the 3-dimensional plots (Figs. 3.10a , 3.10b, 3.10c) indicate for a noticeable change in primary composition towards heavier domination as $N_{\rm e}$ increases across the *knee*. The KASCADE group also reached the similar conclusion using the slope parameter in the modified NKG LDF instead of $s_\perp$ [43]. The 3-dimensional plot over the 2-dimensional $N_{\rm e}$–N_μ curve seems advantageous for the PCR mass composition study so far the KASCADE results are concerned.

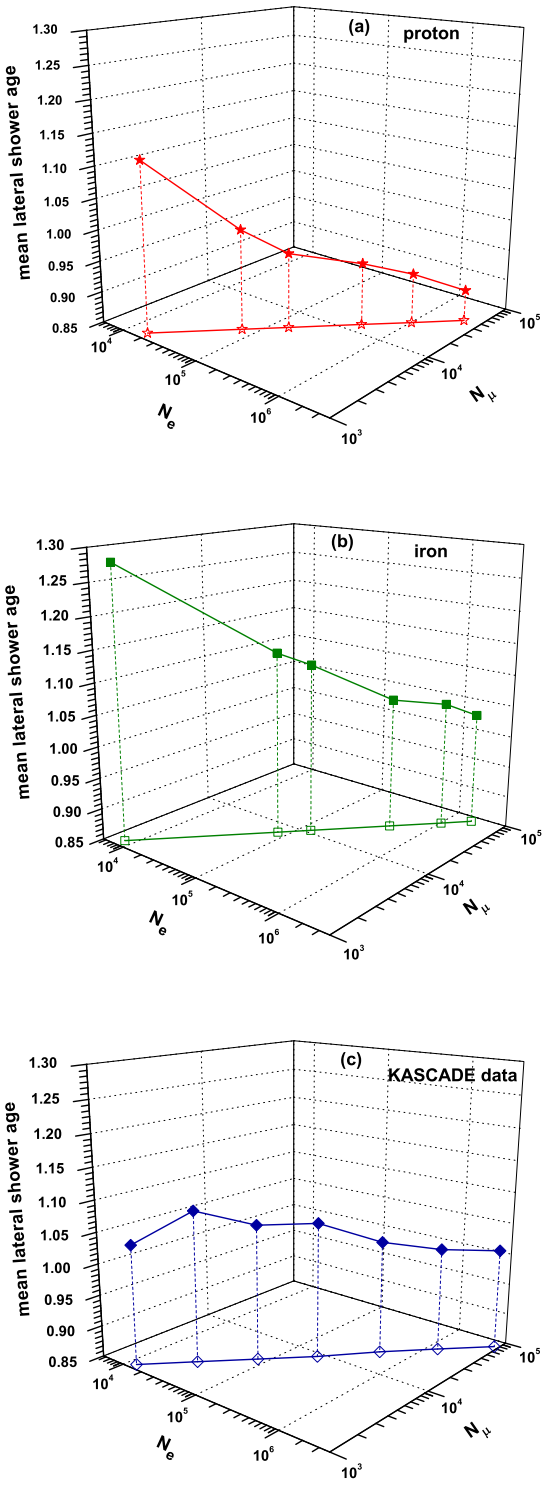

FIGURE 3.10: 3-Dimensional plot using shower size, muon size and lateral shower age parameters at KASCADE level: (a) Pure proton and (b) Pure iron showers, generated using the QGSJet model. KASCADE data are given in (c). Projection on the X–Y plane showing $N_{\rm e}$–N_μ curve.

In the KASCADE experimental data, the error in $s_{\perp}$ estimation remains within 0.06, whereas for the NBU data the error was found to be within 0.04.

3.5 Conclusions

The present work, with particular focus on the $s_{\perp}$ parameter, has yielded the following conclusions.

(1) The $s_{\perp}$ parameter correlates with the stage of shower development on a statistical basis; average of this parameter increases as air showers traverse an increased thickness of atmosphere. This expected behavior is found for two different hadronic interaction models, QGSJet and SIBYLL. The NBU data agree with the simulation and also some early works reported nearly 4 decades ago.

The frequency distributions of differences between $s_{\perp}$ and $s_{\parallel}$ also establish the fact that longitudinal and lateral developments of EAS are strongly correlated through their shape parameters. Such distributions and their central values are found mass sensitive.

(2) The $s_{\perp}$ parameter takes higher values for iron initiated showers as compared to proton showers. This means that lateral distribution of electrons for iron initiated showers is flatter (or older) relative to that of proton showers (younger). The slope of $s_{\perp}$ versus atmospheric depth curve is, however, more or less the same for proton and iron showers. We have also noticed that for mixed primaries the slope of $s_{\perp}$ versus atmospheric depth curve is found smaller compared to pure primary initiated EAS. The observation by the NBU air shower array on this aspect [43] indicates for a dominant lighter (proton) species up to at least around the *knee* energy region.

(3) The $s_{\perp}$ parameter has been found to decrease with the increase of both $N_{\rm e}$ and N_{μ} at least for simulated pure proton. But for simulated iron showers the rate of fall is quite slow, becomes uniform at last in the NBU simulation. However, the variation for experimental data shows a gradual rise instead and, in particular in the KASCADE data (from proton proximity to iron). This clearly indicates a domination of relatively heavy primaries beyond the *knee*. Due to certain limitations of the NBU experiment, the data do not exhibit such distinct signature but

favour a mixed composition across the *knee*.

Many EAS experiments measured the CR mass composition using the conventional approach of implementing the variation of N_μ against N_e, which we have obtained through the 2-dimensional projection on the X–Y plane in each case. Because of a generic feature of EAS development, the total muon number on the ground varies from one species to other and that makes the N_μ as a possible mass sensitive parameter. But, due to limited area covered by muon detectors in an EAS experiment, a truncated size of muons ($N_\mu^{\mathrm{tr.}}$) is obtained. On the other hand, there is no air shower model that can accurately describe N_μ right now (e.g. EPOS gives a little higher N_μ compared to QGSJet and others). Therefore, a precise mass composition study based on N_μ only is still not possible. A comparison among three projected 2-dimensional plots for either the KASCADE or NBU is in accordance with the above prediction involving muons.

(4) The frequency distribution and fluctuation of the $s_\perp$ parameter might be useful to predict the nature of the EAS primary. However, the variation of $\sigma_\perp$ with N_e does not look effective for the measurement of CR mass composition.

Bibliography

[1] B. Rossi and K Greisen, *Rev. Mod. Phys.*, **13**, 240 (1941).

[2] J. Nishimura, and K. Kamata, *Progr. Theor. Phys.*, **5**, 899 (1950).

[3] K. Greisen, *Prog. in Cosmic Ray Physics*, North Holland, Co., Amsterdam, **3** 1 (1956).

[4] K. Kamata and J. Nishimura, *Prog. Theor. Phys. Suppl.*, **6**, 93 (1958).

[5] A. A. Lagutin *et al.*, *Proc. 16th ICRC.*, Kyoto **1**, 18 (1979).

[6] V. V. Uchaikin, *Proc. 16th ICRC.*, **1** 14 (1979).

[7] G. Cocconi, Handbuch der Physik: Cosmic Rays I vol 46/1 (Berlin: Springer) p 215 (1961).

[8] D. J. Bird *et al.*, (Fly's Eye collaboration) *Phys. Rev. Lett.*, **71**, 3401 (1993).

[9] R. U. Abbasi *et al.*, (HIRES collaboration) *Astrophys. J*, **622**, 910 (2005).

[10] J. Nishimura, Handbuch der Physik: Cosmic Rays II vol 46/2 (Berlin: Springer) p 1 (1967).

[11] R. K. Dey, A. Bhadra and J. N. Capdevielle, *J. Phys. G:Nucl. Part. Phys.*, **39** 085201 (2012).

[12] W. D. Apel *et al.*, *Astropart. Phys.*, **24**, 467 (2006).

[13] J. N. Capdevielle, J. Cohen, *J. Phys. G: Nucl. Part. Phys.*, **31**, 507 (2005).

[14] L. G. Dedenko, *et al.*, *Proc. 14th ICRC.*, Munich, **8** 2731 (1975).

[15] M. Hillas and J. Lapikens, *Proc. 15th ICRC.*, Plovdiv, **8** 460 (1977).

[16] T. Antoni *et al.*, (KASCADE Collaboration), *Astropart. Phys.*, **14** 245 (2001).

[17] J. N. Capdevielle and J. Gawin, *J. of Physics G.*, **8**, 1317 (1982).

[18] J. N. Capdevielle and J. Procureur, *Proc. 18th ICRC.*, Bangalore, **11** 307 (1983).

[19] M.F. Bourdeau, J.N. Capdevielle and J. Procureur, *J. Phys.G.*, **6**, 901 (1980).

[20] S. K. Gupta *et al.*, *Nucl. Instrum. Methods.*, A **540**, 311 (2005).

[21] G. Disciascio and T.Di Girolamo, *Astrophys. Space Sci.*, **309**, 537-540 (2007).

[22] K. Greisen, *Ann. Rev. of Nucl. and Part. Science.*, **10**, 63 (1960).

[23] M. Giller, A. Kacperczyk, J. Malinowski, G. TkaczykWandWieczorek, *J. Phys. G: Nucl. Part. Phys.*, **31**, 947 (2005).

[24] F. Nerling, J. Blumer, R. Engel and M. Risse, *Astropart. Phys.*, **24**, 421 (2006).

[25] P. Lipari, *Phys. Rev. D*, **79**, 063001 (2009).

[26] S. Lafebre, R. Engel, H. Falcke, J. Hoerandel, T. Huege, J. Kuijpers and R. Ulrich, *Astropart. Phys.*, **31**, 243 (2009).

[27] F. Schmidt, M. Ave, L. Cazon and A. Chou, *Astropart. Phys.*, **29**, 355 (2008).

[28] D. Gora *et al.*, *Astropart. Phys.*, **24**, 484 (2006).

[29] A. Yushkov *et al.*, *Phys. Rev. D*, **81** 123004 (2010).

[30] W. D. Apel *et al.*, *Astropart. Phys.*, **29**, 412 (2008).

[31] J. N. Stamenov, *Proc. 20th Int. Cosmic Ray Conf.*, (Moscow) vol **8**, p. 258 (1987).

[32] J. N. Capdevielle and P. Gabinski, *J. Phys. G.:Nucl. Part. Phys.*, **16**, 769 (1990).

[33] A. Bhadra, S. K. Sarkar, C. Chakraborty, B. Ghosh and N. Chuodhuri, *Nucl. Instrum. Methods*, A **414** 233 (1998).

[34] T. Antoni *et al.*, *Nucl. Instrum. Methods*, A **513**, 490 (2003).

[35] D. Heck, J. Knapp, J. N. Capdevielle, G. Schatz and T. Thouw, FZKA report-6019 ed. FZK *The CORSIKA Air Shower Simulation Program*, Karlsruhe (1998).

[36] N. N. Kalmykov, S. S. Ostapchenko and A. I. Pavlov, *Nucl. Phys. (Proc. Suppl.)*, B **52**, 17 (1997).

[37] H. Fesefeldt, Report PITHA-85/02 (RWTH Aachen) (1985).

[38] H. J. Drescher *et al.*, *Astropart. Phys.*, **21**, 87 (2004).

[39] W. R. Nelson, H. Hiramaya, D. W. O. Rogers, Report SLAC 265, (1985).

[40] R. S. Fletcher, T. K. Gaisser, P. Lipari and T. Stanev, *Phys.Rev. D*, textbf50, 5710 (1994).

[41] National Aeronautics and Space Administration (NASA), U. S. Standard Atmosphere, Tech. Rep. NASA-TM-X-74335 (1976)

[42] J. Knapp, and D. Heck, Tech. Rep. 5196B, Kernforschungszentrum Karlsruhe (1993).

[43] A. Bhadra, *Pramana: J. Phys.*, **52**, 2 (1999).

[44] S. Miyake, *et al.*, *Proc. of ICRC.*, **13**, p. 171 (1979).

[45] J. N. Capdevielle and F. Coheh, *J. Phys. G: Nucl. Part. Phys.*, **31**, 507 (2005).

[46] J. N. Capdevielle and F. Cohen, *J. Phys. G: Nucl. Part. Phys.*, **31**, 1413 (2005).

[47] R. K. Dey and A. Bhadra, *Astropart. Phys.*, **44**, 68 (2013).

[48] Ph. Catz *et al.*, *in: Proc. of ICRC.*, (Denver, USA) vol.**4**, 2495 (1973).

[49] H. Ulrich *et al.*, *Nucl. Phys. B*, **175**, 273 (2008).

[50] H. Ulrich *et al.*, *Nucl. Phys. B*, **196**, 80 (2009).

[51] W. D. Apel *et al.*, *Astropart. Phys.*, **29**, 412 (2008).